

Entanglement generation across exceptional points in two-qubit open quantum system – the role of initial states

B. A. Tay*

*School of Mathematical Sciences, Faculty of Science and Engineering,
University of Nottingham Malaysia, Jalan Broga, 43500 Semenyih, Selangor, Malaysia*

Yee Shean H'ng

*Department of Mechanical, Materials and Manufacturing Engineering,
Faculty of Science and Engineering, University of Nottingham Malaysia,
Jalan Broga, 43500 Semenyih, Selangor, Malaysia*

(Dated: August 25, 2025)

We study an open quantum system of two qubits that are coupled by swapping interaction. Using the coupling strength between the qubits as a time scale, the Liouvillian of the system has exceptional points that depend on the disparity between the decay rates of the qubits. We find that the configuration of the initial states plays an important role in deciding the character of the entanglement dynamics at the initial stage of evolution. Depending on whether or not the initial excitations of the qubits can be swapped by the interaction that couples them, a change in the total decay rate can be either consistently unfavorable to entanglement generation, or shift the dynamics from hindering to enhancing entanglement generation, or vice versa, as the system traverses the exceptional points. The shift could also occur in a wide range of mixed states. We clarify the origin of the behavior in this work.

I. INTRODUCTION

Recently, non-Hermitian quantum systems [1–3] have been effectively realized in the laboratories, for example, in three-level superconducting transmon circuits [4, 5], two-level atoms in cavity [6], photonic systems [7, 8], optical systems [9, 10] and mechanical systems [11, 12]. The development provides avenue to study non-Hermitian degeneracy [13, 14] that occurs at the exceptional points in the parameter space of the systems. At the exceptional points, the eigenvalues and the eigenvectors of the non-Hermitian Hamiltonian coalesce. In contrast to Hermitian degeneracy where the eigenvectors can still be chosen to be orthogonal, non-Hermitian degeneracy leads to a Jordan block structure of the Hamiltonian, giving rise to generalized eigenvectors [15–17].

Initial studies on non-Hermitian degeneracy focused on the Hamiltonian level [1, 3]. Later on, Liouvillian exceptional points were investigated [18–20]. On the Liouvillian level, the quantum jump formalism offers insight in clarifying the differences between the exceptional points structure in non-Hermitian Hamiltonian and its related Liouvillian with jump terms [21].

Contrary to the common belief that dissipation is unfavorable to quantum processes, interesting phenomena were reported when the systems were close to the vicinity of non-Hermitian exceptional points, such as speeding up of entanglement generation [22, 23], topological energy transfer [24, 25], enhanced sensing [26, 27], or when the dynamics encircles the exceptional points [28], leading to chiral state transfers [29, 30] and enhancement of quantum heat engine [31].

A recent study of the effective non-Hermitian Hamiltonian of two qubits derived from three-level system subjected to resonant drives, revealed that at the vicinity of the exceptional point which is decided by the driving amplitude [22], a weak coupling between the qubits could greatly enhance entanglement generation in a very short time scale. The general entanglement dynamics of this system was studied later [32]. Different types of entanglement dynamics can be induced by exceptional points through adjustment of the driving amplitude [33].

Motivated by this result, we investigate a much simpler system of two qubits coupled by swapping interaction, and explore the role of initial states on entanglement generation while the system traverses exceptional points. We find that the initial states, depending on whether or not their initial excitations can be swapped by the interaction that couples the two qubits, play an essential role in deciding the extent of entanglement generation at the initial stage of the evolution. For initial conditions with one of the qubits excited, the excitation can be swapped between the two qubits. Then an increase in decay rate consistently hinders entanglement generation as the system crosses over the exceptional points. On the other hand, when both qubits are initially excited, the swapping of excitations does not bring observable changes to the state. Now an increase in the decay rate surprisingly enhances entanglement generation at the initial stage of the dynamics. However, when the system crosses over the exceptional point, the dynamics turns over into impeding entanglement generation. This is contrary to the common belief that an increase in decay rate is in general unfavorable to entanglement generation.

Though arising from different origins, the effect reminds us of the noise-assisted energy transport [34–36] discussed recently in quantum networks and light-

* BuangAnn.Tay@nottingham.edu.my

harvesting complexes, where dissipation can occasionally be advantageous to energy transport. Here, our focus is on entanglement generation. We clarify the origin of the effect in subsequent sections.

The model of two qubits coupled via the swapping interaction as well as its extension to non-Hermitian qubits, a chain of qubits and their variants has been used widely to model various quantum processes, such as the dynamics of quantum entanglement [6, 22, 32, 33], energy transport in quantum networks and photosynthetic systems [34–36], efficiency of quantum heat engines [37, 38], quantum sensing in photonic systems [10, 22, 39], exciton transfer in molecular systems [40], etc. Here, our focus is on the behavior of entanglement generation between two coupled qubits under different initial conditions. Since entanglement is an important resource in quantum information processing [41], our results provide a different perspective on the interplay between dissipation and entanglement generation, where dissipation could be beneficial to entanglement generation under some initial states.

In Sec. II, we introduce the quantum master equation of two qubits and clarify the structure of its exceptional points in the subspace spanned by the X state. Then we elucidate the behaviors of the dynamics with either one or two qubits excited as the initial conditions in Sec. III and IV, respectively. We show that the time evolution under different initial conditions exhibits different behaviors when the decay rate changes across the exceptional points. A mixture of different initial conditions is considered in Sec. V. We then summarize our results in Sec. VI.

II. TWO-QUBIT OPEN QUANTUM SYSTEM

The quantum master equation we look into is a Gorini-Kossakowski-Sudarshan-Lindblad (GKSL) equation with completely positive evolution [42, 43]. Variants of the systems had been previously used to study entanglement sudden death in various setups [44, 45]. However, the behavior of entanglement generation across exceptional points has not been fully explored. Previous studies [22, 32, 33] considered a model with resonant drives and qubits with equal decay rates. Here, we exclude resonant drives and permit unequal decay rates of the qubits to study the effects on entanglement generation.

We consider two identical qubits with effective energy ω_0 , using the units $\hbar = 1$. They are coupled by a swapping interaction with strength J [22],

$$H = \frac{\omega_0}{2}\sigma_z + \frac{\omega_0}{2}\mu_z + J(\sigma_+\mu_- + \sigma_-\mu_+), \quad (1)$$

where σ_z and μ_z label the z -component of the Pauli matrices for the first and second qubit, respectively, and $\sigma_{\pm} \equiv (\sigma_x \pm i\sigma_y)/2$ are the creation and annihilation operators of the first qubit, with similar definitions μ_{\pm} for the second qubit. The interaction can be realized between two identical two-level atoms interacting with a cavity mode [46], or between two non-Hermitian qubits

in a superconducting circuit [6]. We consider two qubits free from resonant drives. The first and second excited qubits relax to their ground states with decay rates γ_1 and γ_2 , respectively. In the interaction picture, the two-qubit reduced dynamics is described by the GKSL master equation

$$\frac{\partial \rho}{\partial t} = -K\rho, \quad (2)$$

where

$$\begin{aligned} K\rho = & i[J(\sigma_+\mu_- + \sigma_-\mu_+), \rho] \\ & - \frac{\gamma_1}{2}(2\sigma_-\rho\sigma_+ - \sigma_+\sigma_-\rho - \rho\sigma_+\sigma_-) \\ & - \frac{\gamma_2}{2}(2\mu_-\rho\mu_+ - \mu_+\mu_-\rho - \rho\mu_+\mu_-). \end{aligned} \quad (3)$$

The two-qubit density operator, ρ , is a 4×4 positive semidefinite Hermitian matrix with trace 1. In the following discussion, we will restrict our attention to the subspace spanned by the so-called X state [44],

$$\rho_X = \begin{pmatrix} a & 0 & 0 & h \\ 0 & b & m & 0 \\ 0 & m^* & c & 0 \\ h^* & 0 & 0 & d \end{pmatrix}, \quad (4)$$

with the normalization condition $a + b + c + d = 1$, and $*$ denotes complex conjugate. The X state remains in this subspace under the evolution of the reduced dynamics (2). Introducing a dimensionless time

$$\tau \equiv 2Jt, \quad (5)$$

and defining three parameters,

$$x \equiv b + c, \quad (6)$$

$$y \equiv b - c, \quad (7)$$

$$z \equiv m - m^*, \quad (8)$$

the equation of motion of the matrix elements together with their solutions is listed in App. B. We further introduce a rescaled total decay rate

$$\gamma \equiv \frac{1}{4J}(\gamma_1 + \gamma_2), \quad (9)$$

and a rescaled disparity between the two qubits' decay rates

$$\kappa \equiv \frac{1}{4J}(\gamma_2 - \gamma_1). \quad (10)$$

Because $\gamma_1, \gamma_2 \geq 0$, the following constraint must be satisfied by the rescaled quantities,

$$|\kappa| \leq \gamma. \quad (11)$$

Two of the parameters, $m + m^*$ and h (and its complex conjugate), evolve independently from each other, see Eqs. (B1)-(B7) for the details. Hence, we focus on the subspace formed by the five parameters a, x, y, z and d .

The generator of evolution for the matrix elements of this subspace has the eigenvalues,

$$\begin{aligned} \lambda_0 &= 0, & \lambda_1 &= -2\gamma, & \lambda_2 &= -\gamma, \\ \lambda_3 &= -\gamma - \Delta, & \lambda_4 &= -\gamma + \Delta, \end{aligned} \quad (12)$$

see App.C, where

$$\Delta \equiv \sqrt{\kappa^2 - 1} \quad (13)$$

determines the behavior of the dynamics. When $\kappa = \pm 1$, it follows that $\Delta = 0$. Then two of the eigenvalues in Eq. (12) coalesce into $-\gamma$ to give two third-order exceptional points in this subspace. The corresponding eigenvectors are listed in App. C. There, it is also shown that the three eigenvectors indeed coalesce at the exceptional points.

The solutions exhibit similar behaviors to a damped oscillator discussed in App. A. Using an analogy to the damped oscillator described there, the evolution of the qubits is critically damped at the exceptional points. As $|\kappa|$ increases from below 1, the motion develops from oscillatory (underdamped) to purely exponential decay (overdamped), after crossing over the exceptional point at $|\kappa| = 1$.

The two regions separated by the exceptional points are related to parity-time (PT) symmetry phase and spontaneously broken symmetry phase [2, 7, 8]. PT symmetry could arise when there is a balance between the gain and loss components in non-Hermitian systems. In the present model, it is convenient to consider PT symmetry in the subspace of the correlation functions $\langle \sigma_{\pm} \mu_{\pm} \rangle$ of the two qubits. We present the details in App. D. By absorbing an overall exponential factor into the correlation functions [7], we can bring the model with two decay channels into a form that is balanced in gain and loss (see the $\pm i\kappa$ terms along the diagonal of the time evolution matrix (D2)); hence, the term “passive” PT symmetry. The $|\kappa| < 1$ region that exhibits oscillatory motion is in the PT -symmetry phase, whereas the $|\kappa| > 1$ region that shows purely exponential decay is in the spontaneously broken PT -symmetry phase. The exceptional points are the critical points of the phase transitions. In the symmetry broken phase, the time evolution operator remains PT symmetric. However, the solutions no longer satisfy the symmetry [2], see Eq. (D8) and the discussion in App. D for the details.

In this work, our main focus is the entanglement generation dynamics at the initial stage of the time evolution. We use concurrence C [47] as a measure of entanglement between the qubits. In this model, it can be determined by $C = 2 \max(0, \sqrt{\lambda_1} - \sqrt{\lambda_2} - \sqrt{\lambda_3} - \sqrt{\lambda_4})$, where λ_i 's are the eigenvalues of $\rho(\sigma_y \mu_y) \rho^* \cdot (\sigma_y \mu_y)$ arranged in descending order. For the X state (4), the concurrence has

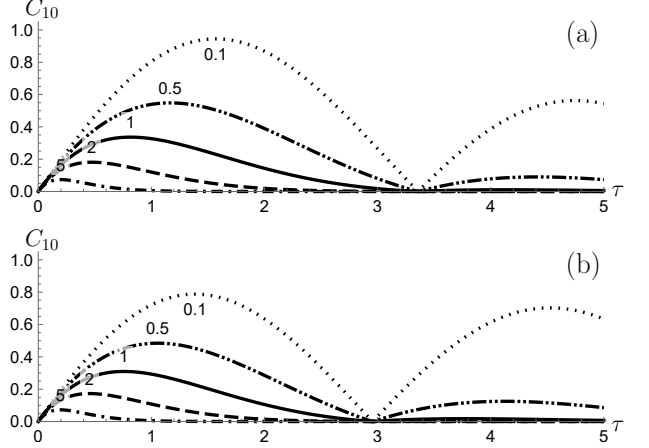


FIG. 1. Time evolution of concurrence for (a) $\kappa = 0.1$ and (b) $\kappa = -0.1$ with initial condition $|10\rangle$. The values of γ are shown on the curves.

a simple expression [45],

$$C = 2 \max(0, |m| - \sqrt{ad}, |h| - \sqrt{bc}) . \quad (14)$$

III. INITIAL CONDITION WITH SINGLY EXCITED QUBIT

For a non-entangled initial condition $|10\rangle$, the density matrix $\rho_{10} \equiv |10\rangle\langle 10|$ begins with $b_0 = 1$, while the rest of the parameters are zero, $a_0 = c_0 = d_0 = h_0 = m_0 = m_0^* = 0$, or equivalently, $x_0 = 1 = y_0$ and $z_0 = 0$. We define the concurrence as C_{10} , consistent with the notation ρ_{10} for the first qubit excited state. In this situation, because a and h always vanish, the concurrence depends only on the magnitude of z ,

$$C_{10}(\tau) = |z| . \quad (15)$$

For $1 < |\kappa|$, z (B13) can be written as,

$$z = e^{-\gamma\tau} \frac{i}{\Delta^2} \left(\kappa \cosh(\Delta\tau) - \kappa + \Delta \sinh(\Delta\tau) \right) . \quad (16)$$

A corresponding expression exists for $-1 < \kappa < 1$ when we introduce a parameter $\bar{\Delta} \equiv \sqrt{1 - \kappa^2}$ (D5) defined from $\Delta = i\bar{\Delta}$, and make use of the identities of hyperbolic functions with imaginary arguments to get functions with oscillatory behaviors.

For fixed κ , Fig. 1 (with $\kappa = 0.1$) shows that maximum concurrence occurs when γ assumes its smallest value at $\gamma = \kappa$, in view of the constraint $|\kappa| \leq \gamma$ (11). As γ increases from 0.1 to infinity, the maximum concurrence reduces steadily and approaches 0. The monotonic behavior can be understood as follows. Since the first qubit does not decay ($\gamma_1 = 0$) in the $\gamma = \kappa$ situation, there always remains a larger population of the state $|10\rangle$ in the $\gamma = \kappa$ compared to the $\gamma > \kappa$ situation. Therefore, there is a higher probability for the state $|10\rangle$ to swap into $|01\rangle$

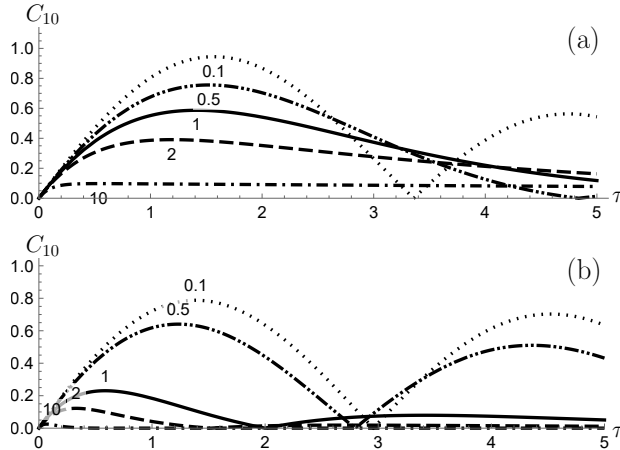


FIG. 2. Time evolution of concurrence when we set $\gamma = |\kappa|$ with initial condition $|10\rangle$. The values of γ are shown on the curves. (a) $\kappa > 0$ so that γ_1 is always 0 and $\gamma = \gamma_2$. (b) $\kappa < 0$ so that γ_2 is always 0 and $\gamma = \gamma_1$. The system is critically damped at $|\kappa| = 1$.

through the coupling between the qubits. Quantum correlation can then be established between the states to generate the maximally entangled Bell states $|10\rangle \pm |01\rangle$. This explains the maximum value of concurrence for the $\gamma = \kappa$ curve.

When total decay rate increases, entanglement generation of Bell's states needs to compete with the higher decay rates of $|10\rangle$ and $|01\rangle$ to the ground state $|00\rangle$. This results in a lower value of the maximum concurrence generated for the $\gamma > \kappa$ situation. This is revealed in Fig. 1(a) where the $\gamma = \kappa$ curve envelopes all other $\gamma > \kappa$ curves.

Similar behaviors are observed when we fix κ at a negative value, depicted in Fig. 1(b) for $\kappa = -0.1$. The main difference between Figs. 1(a) and 1(b) is that the maximum concurrence achieved with negative κ is less than that with positive κ . This is because for $\gamma = -\kappa$, we now have $\gamma_2 = 0$. A further increase in the total decay rate $\gamma = \gamma_1$ will reduce the initial pool of $|10\rangle$ population, thus slowing down the generation of Bell states. Hence, the maximum concurrence achieved in the negative- κ curves are less than the positive- κ curves. Apart from this, Fig. 1(b) shows that the $\gamma = -\kappa$ curve envelopes all other $\gamma > -\kappa$ curves. We also notice that the revival time of concurrence for negative- κ is shorter than that for positive- κ . In both situations concurrence approaches 1 as $\gamma \rightarrow 0$ when the system returns to unitary.

In Figs. 2(a) and 2(b) we plot the evolution for $\gamma = \kappa$ and $\gamma = -\kappa$, respectively, for a few γ 's. As γ varies from 0.1 to 10, the system crosses over the exceptional points located at $\kappa = \pm 1$. We observe the occurrence of similar differences between Figs. 2(a) and 2(b) with those between Figs. 1(a) and 1(b), that is, (i) monotonic reduction in the maximum concurrence for larger γ , (ii) smaller maximum concurrence achieved in negative κ curves compared to positive κ curves, (iii) small

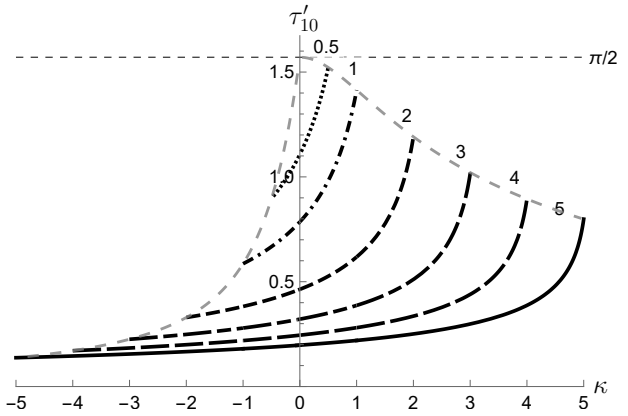


FIG. 3. Initial condition $|10\rangle$. The instant (τ'_{10}) when the first maximum concurrence for fixed γ occurs. The value of γ ranges from 0.5 to 5, as shown at the end of the curves. κ satisfies the constraint $|\kappa| \leq \gamma$ (11). Dashed gray lines are the enveloping curves satisfying the condition $\gamma = |\kappa|$.

revival time for concurrence in negative κ curves, and (iv) the approach of concurrence to 1 as γ vanishes when the system becomes unitary.

If we initiate a setup with the second qubit excited $|01\rangle$, the concurrence can be deduced from C_{10} (15)-(16) with a reflection in the parameter $\kappa \leftrightarrow -\kappa$, while γ remains the same. The consequence is a switching of the results between Figs. 1(a) and 1(b), i.e., now Fig. 1(a) applies to negative κ curves, whereas Fig. 1(b) applies to positive κ curves. Therefore, it is sufficient that we focus on the initial condition $|10\rangle$ to understand the dynamics. Furthermore, since the $\gamma = |\kappa|$ curve envelopes all other $\gamma > |\kappa|$ curves for fixed κ , in the following we will only consider the $\gamma = |\kappa|$ situation when analyzing the maximum concurrence generated across the exceptional points.

Next, we investigate the instant t' at which the system first reaches maximum concurrence. It corresponds to the rescaled time $\tau' = 2Jt'$. It is the time when the first peaks in Figs. 1(a), 1(b), 2(a) and 2(b) occur. For the initial condition $|10\rangle$, we label the instant as τ'_{10} . The time derivative of the concurrence $dC_{10}/d\tau$ is given in App. E, see Eq. (E1). Solving $dC_{10}/d\tau|_{\tau=\tau'_{10}} = 0$ for the first concurrence maximum, we obtain two expressions for $1 < |\kappa|$ (E4) and $-1 < \kappa < 1$ (E5) for the overdamped and underdamped region, respectively. The results are plotted in Fig. 3. The curves show the variation of τ'_{10} with κ for fixed value of γ (indicated on the curves). The longest duration occurs at the right end of each curve when $\kappa = \gamma$, a result that can be deduced by inspecting Fig. 2(a). It is shown at the end of App. E that the overall longest time to achieve maximum concurrence is $\tau'_{10,\max} = \pi/2$, which occurs in the limit $\gamma \rightarrow 0$, indicated by the horizontal dashed-line in Fig. 3. This implies that for the initial condition $|10\rangle$, in all the curves maximum

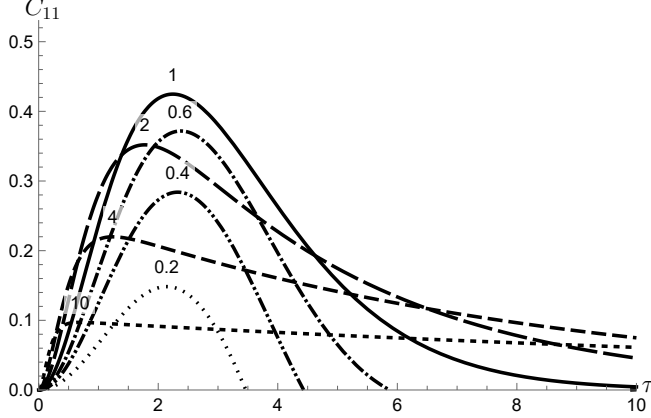


FIG. 4. $C_{11}(\tau)$ with $\kappa = \gamma$. The values of γ are shown on the curves. Beginning with $\gamma = 0.2$, at first the increase of dissipation enhances entanglement generation. After reaching a maximum on the curve $\gamma = 1.02$ (almost overlap with the curve $\gamma = 1$, not shown in the figure), a further increase in dissipation starts hindering entanglement generation.

concurrence is reached before

$$t'_{10,\max} = \frac{\pi}{4J}. \quad (17)$$

In Fig. 3, the enveloping dashed grey line on the right (left) quadrant that connects the right (left) end of the curves gives the instant of the first maximum concurrence at $\gamma = \kappa$ ($\gamma = -\kappa$), respectively. A steady and monotonic reduction of the time with the increase of $|\kappa|$ is evident in the figure. These curves are the counterparts to a similar curve plotted in Fig. 5(b) for a different initial condition, to be considered in the next section.

IV. INITIAL CONDITION WITH TWO EXCITED QUBITS

For the initial condition with both qubits excited $|11\rangle$, the initial values of the density matrix $\rho_{11} \equiv |11\rangle\langle 11|$ are $a_0 = 1$, while $b_0 = c_0 = d_0 = h_0 = m_0 = m_0^* = 0$. Since h always vanishes, the concurrence is

$$C_{11}(\tau) = \max(0, |z| - 2\sqrt{ad}), \quad (18)$$

where we define the concurrence in accordance to the indices of the initial state ρ_{11} . From Eqs. (B8), (B13) and (B14), we then obtain for $1 < |\kappa|$,

$$C_{11}(\tau) = 2e^{-\gamma\tau} \left[\frac{2|\kappa|}{\kappa^2 - 1} \sinh^2 \left(\frac{\Delta}{2}\tau \right) - \sqrt{\left(1 - e^{-\gamma\tau}\right)^2 - \frac{4\kappa^2 e^{-\gamma\tau}}{\kappa^2 - 1} \sinh^2 \left(\frac{\Delta}{2}\tau \right)} \right]. \quad (19)$$

Notice that the concurrence is reflection symmetric with respect to $\kappa \leftrightarrow -\kappa$. Therefore, we will consider only positive κ in the following discussion. A corresponding

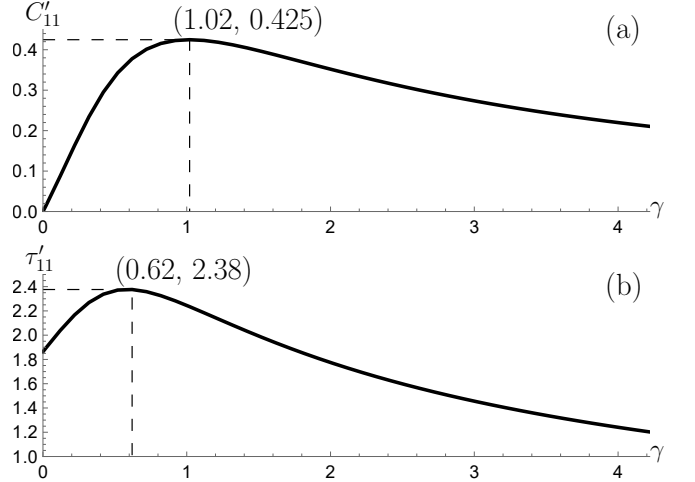


FIG. 5. (a) The maximum value of $C_{11}(\tau)$, C'_{11} , is plotted as a function of $\gamma (= \kappa)$. The coordinates of the extremum are shown, which are very close to the exceptional point, $\kappa = 1$. (b) The time when the first concurrence maximum is reached, τ'_{11} , is plotted as a function of $\gamma (= \kappa)$.

expression can be obtained for $-1 < \kappa < 1$ in a similar way to C_{10} already discussed at the end of the first paragraph of the last section.

Similar to Fig. 1 in the previous section, the $\gamma = \kappa$ curve envelops all other $\kappa < \gamma$ curves within it. Hence, it is sufficient for our purpose to study the time evolution of $\gamma = \kappa$, as depicted in Fig. 4. The curves for a few γ on both sides of the exceptional point are plotted. Note that for the underdamped cases $\gamma < 1$, there is entanglement sudden death [44, 45], i.e., the concurrence vanishes abruptly in finite time. Because of the definition of concurrence (18) that chooses the greater value between 0 and $|z| - 2\sqrt{ad}$, the oscillatory behaviors in the underdamped motion are absent from Fig. 4 because they occur in the $|z| - 2\sqrt{ad} < 0$ region.

The first maximum of concurrence achieved in each curve, C'_{11} , is plotted in Fig. 5(a) as a function of γ , whereas the instant when the first maximum occurs, τ'_{11} , is plotted in Fig. 5(b). We observe an interesting behavior in the change of maximum concurrence in Fig. 5(a). When the total decay rate increases from 0, the concurrence first increases to an extremum value of $C'_{11} = 0.425$ around $\gamma = 1.02$, after it crosses over the exceptional point at $\gamma = \kappa = 1$ into the overdamped region. Here in the underdamped region, the increase in dissipation enhances entanglement generation. The longest duration taken by this process is $\tau'_{11} = 2.38$, see Fig. 5(b). Hereafter, a further increase in γ turns the dynamics from enhancing to hindering entanglement generation. In other words, there is dissipation-assisted entanglement generation for the two-excited-qubits initial condition. Similar phenomena were found in quantum networks and light-harvesting complexes [34–36] where under right condition noise could be assisting energy transport, though

the process has a different physical origin from the one considered here.

We can understand how dissipation could assist in entanglement generation as follows. The condition $\gamma = \kappa$ implies that the first qubit does not decay $\gamma_1 = 0$. Hence, decay is solely due to the second qubit, $\gamma = \gamma_2$. When we start with a small decay rate, the initial condition with both qubits excited $|11\rangle$ does not give much room for the formation of Bell's states, because of the relatively low population of the newly formed $|10\rangle$ state, which should first swap into $|01\rangle$ before Bell's states could be formed. As the dissipation rate gradually increases, the decay of the second qubits produces higher enough population of $|10\rangle$. This creates higher probability for the swapping of $|10\rangle$ into $|01\rangle$, and thus enhancing entanglement generation between the qubits. This is an example of dissipation-assisted entanglement conditioned by the initial state. Since this is a two-step process, i.e., first decay and then swapping, it is not surprising that for a wide range of γ , the time taken to generate maximum concurrence in Fig. 5(b) is generally longer than the corresponding time required for the one excited qubit initial condition in Fig. 3, where in the latter it is always less than $\pi/2$. With the same reasoning, Fig. 5(a) shows that the maximum concurrence in this case is also considerably less than the case achieved with initial condition $|10\rangle$ in Figs. 2(a) and 2(b) because of the higher loss in populations caused by the longer duration required to generate entanglement.

The maximum concurrence increases steadily until κ is close to the exceptional points where entanglement generation becomes saturated. After crossing over the exceptional points into the overdamped region, further increase in the total decay rate ($\gamma = \gamma_2$) starts to reduce the population of $|01\rangle$ needed to form entangled states after the swapping. Now dissipation begins to hinder entanglement, as commonly occurs in most systems. Thereafter, the maximum concurrence decreases gradually as γ increases further.

Quantum entanglement, quantified by concurrence considered in this work, is a form of quantum correlation. One might wonder whether the extremum behavior shown in Figs. 5(a)-(b) would also show up in the correlation functions of two qubits $\langle\sigma_i\mu_j\rangle \equiv \text{tr}(\sigma_i\mu_j\rho)$, where $i, j = x, y, z$. Using $\langle\sigma_x\mu_y\rangle = -i(z - h + h^*)$ (F2) as an example, in App. F we show that the extremum behavior indeed occurs in the two excited qubits initial condition, see Fig. 7(a). However, since the concurrence C_{11} (18) is also affected by the diagonal components of the density matrix, i.e., a and d , the extrema in the two quantities do not occur at the same value of γ . Furthermore, the instant when the first maximum of the correlation function is achieved is monotonously reducing with γ , see Fig. 7(b). It behaves differently from the corresponding time in concurrence, see Fig. 5(b). Therefore, the correlation functions cannot be used as substitutes of concurrence to identify the maximum of entanglement.

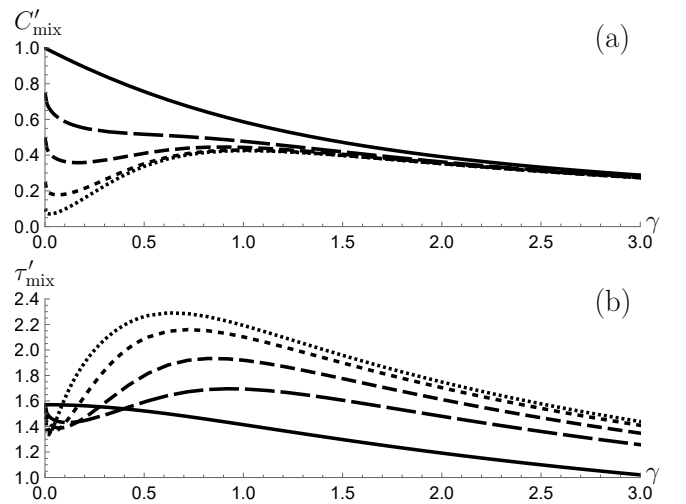


FIG. 6. Mixed state $\rho_{\text{mix}}(\alpha)$. (a) Maximum concurrence is plotted as a function of $\gamma(= \kappa)$. (b) The time when the first maximum concurrence occurs. The values of α are, 1 (solid), 0.75 (long-dashed), 0.5 (medium-dashed), 0.25 (short-dashed), and 0.1 (dotted) curves, respectively.

V. MIXTURE OF STATES

We can form a mixture of states by a convex sum of the initial conditions of the two qubits, which we define as

$$\rho_{\text{mix}}(\alpha) \equiv \alpha\rho_{10} + (1 - \alpha)\rho_{11}, \quad (20)$$

where $0 \leq \alpha \leq 1$. This state has the initial condition $a_0 = 1 - \alpha$, $b_0 = x_0 = y_0 = \alpha$, while the rests are zero.

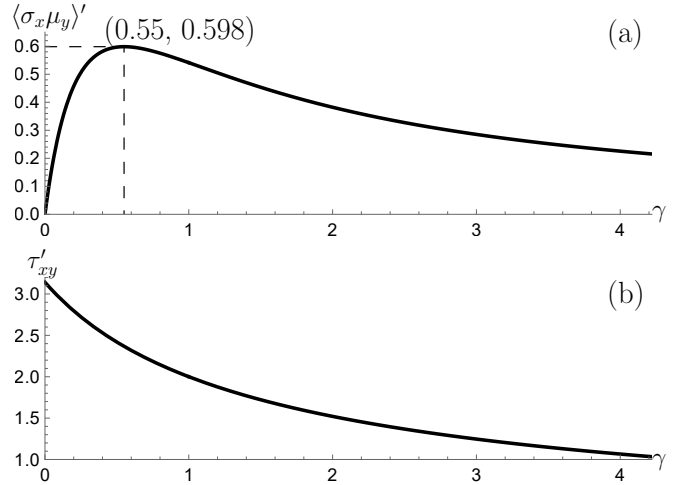


FIG. 7. (a) The maximum value of the correlation function, $\langle\sigma_x\mu_y\rangle'$, is plotted as a function of $\gamma(= \kappa)$. The extremum occurs far from the exceptional point, $\kappa = 1$. (b) The instant when the first maximum of $\langle\sigma_x\mu_y\rangle'$ is reached, τ'_{xy} , is plotted as a function of $\gamma(= \kappa)$.

The concurrence has the same expression as Eq. (18), though with different parameters listed in App. G, see Eqs. (G1)-(G3).

The values of the first maximum concurrence in this case, which we denote by C'_{mix} , which can be achieved for various α and the time taken, τ'_{mix} , are plotted in Figs. 6(a) and 6(b), respectively, as a function of the total decay rate γ for the condition $\kappa = \gamma$. Here we only consider positive κ for simplicity to show the general features of entanglement dynamics with $\rho_{\text{mix}}(\alpha)$ as the initial condition.

By comparing Figs. 6(a) and 6(b) with Figs. 5(a) and 5(b) ($\alpha = 0$), respectively, we find a competition between the two entanglement dynamics discussed in the previous sections. Focusing on Fig. 6(a), we begin with the state ρ_{10} (solid curve with $\alpha = 1$). As α reduces from 1, we first observe that the maximum concurrence reduces steadily over a wide range of γ until the weight of the state ρ_{11} becomes prominent enough to bring noticeable changes to the dynamics. This occurs approximately below $\alpha < 0.75$ (long-dashed curve). Now in the underdamped region $\gamma = \kappa < 1$ a hollow starts to form which becomes obvious around $\alpha = 0.5$ (medium-dashed curve), signifying a shift from a mode of entanglement hindrance to a mode of entanglement enhancement by dissipation. Now, maxima in the concurrence curves start to appear, and there exists optimal dissipation rate for entanglement generation over a wide range of mixed states. Fig. 6(b) shows that the time needed to achieve maximum concurrence generally increases as the weight of ρ_{11} increases, consistent with the discussion in the previous section. Here, optimal entanglement generation is compromised by the need of a longer interval to achieve its maximum.

VI. CONCLUSION

We have shown that the interplay between the configuration of the initial states and the interaction between the two qubits is crucial in deciding the character of entanglement dynamics at the initial stage of evolution in a two-qubit open quantum system. Contrary to the common belief that dissipation is in general detrimental towards entanglement generation, for certain initial states an increase in the total decay rate can instead favor entanglement generation.

We note that the configuration that shows the crossover behavior requires one of the excitations to first relax before entanglement can be generated. This causes the system to undergo dissipation throughout a relatively longer time scale of the order of the qubit's decay time. As a result, the overall maximum entanglement achieved is relatively less. In summary, we have clarified the general features required and the regions the system must lie in to optimize entanglement generation across the exceptional points in the two-qubit open quantum system. Since dissipation is inevitable in quantum processes, our results provide a different perspective on the effects of

dissipation to entanglement dynamics.

ACKNOWLEDGMENTS

We are grateful for the support of the Fundamental Research Grant Scheme (FRGS), Grant No. FRGS/1/2020/STG07/UNIM/02/01, by the Ministry of Higher Education Malaysia (MOHE). Y.S.H. is supported as a Graduate Research Assistant (GRA) under this grant.

Appendix A: Classical damped oscillator

The position of a damped oscillator obeys the equation $m\ddot{x} + \gamma\dot{x} + kx = 0$, where γ and k denotes the damping and the spring constant, respectively. We can turn the equation into two simultaneous equations. In matrix form, they are

$$\dot{\mathbf{X}} = \mathbf{K} \cdot \mathbf{X}. \quad (\text{A1})$$

where

$$\mathbf{X} \equiv \begin{pmatrix} x \\ v \end{pmatrix} \quad (\text{A2})$$

and

$$\mathbf{K} = \begin{pmatrix} 0 & 1 \\ -k/m & -\gamma/m \end{pmatrix} \quad (\text{A3})$$

with the solution $\mathbf{X}(t) = e^{\mathbf{K}t} \cdot \mathbf{X}$. The eigenvalue equation $\mathbf{K} \cdot \mathbf{v} = \tilde{\lambda} \mathbf{v}$ has the solutions (we set $m = 1$)

$$\tilde{\lambda}_{\pm} = -\frac{1}{2}(\gamma \pm \tilde{\Delta}), \quad (\text{A4})$$

where

$$\tilde{\Delta} \equiv \sqrt{\gamma^2 - 4k}, \quad (\text{A5})$$

and the eigenvectors

$$\mathbf{v}_{\pm} = \begin{pmatrix} \tilde{\lambda}_{\mp} \\ -k \end{pmatrix}. \quad (\text{A6})$$

The damped oscillator can show three types of motion. The motion is oscillatory when $\gamma^2 < 4k$, where $\tilde{\Delta}$ is imaginary, i.e., the oscillator is underdamped. The position x decays exponentially when $\gamma^2 > 4k$, where $\tilde{\Delta}$ is real. The oscillator is then overdamped. Critical damping occurs at $\gamma^2 = 4k$, when $\tilde{\Delta} = 0$.

The eigenvalues and eigenvectors coalesce at the exceptional point, which occurs at $\gamma^2 = 4k$. This corresponds to critical damping. The eigenvalues coalesce to

$$\tilde{\lambda}_c \equiv \tilde{\lambda}_+ = \tilde{\lambda}_- = -\frac{\gamma}{2}. \quad (\text{A7})$$

At the exceptional point, the first eigenvector

$$\mathbf{v}_0 = \begin{pmatrix} 1 \\ -\tilde{\lambda}_c \end{pmatrix} \quad (\text{A8})$$

satisfies the eigenvalue equation

$$\mathbf{K} \cdot \mathbf{v}_0 = \tilde{\lambda}_c \mathbf{v}_0. \quad (\text{A9})$$

To complement \mathbf{v}_0 , we need to consider the generalized eigenvalue equation (A9),

$$\mathbf{K} \cdot \mathbf{v}_1 = \tilde{\lambda}_c \mathbf{v}_1 + \mathbf{v}_0. \quad (\text{A10})$$

\mathbf{v}_0 and \mathbf{v}_1 are the generalized eigenvectors of \mathbf{K} at the exceptional point. There is a great deal of freedom in the choice of the second generalized eigenvector

$$\mathbf{v}_1 = \begin{pmatrix} a \\ -1 - a\tilde{\lambda}_c \end{pmatrix}, \quad (\text{A11})$$

for real a .

Appendix B: Solutions to equations of motion

The equations of motion of the matrix elements in the X state (4) are

$$\dot{a} = -2\gamma a, \quad (\text{B1})$$

$$\dot{x} = 2\gamma a - \gamma x + \kappa y, \quad (\text{B2})$$

$$\dot{y} = 2\kappa a + \kappa x - \gamma y + iz, \quad (\text{B3})$$

$$\dot{z} = -\gamma z + iy, \quad (\text{B4})$$

$$\dot{d} = \gamma x - \kappa y, \quad (\text{B5})$$

$$\dot{m} + \dot{m}^* = -\gamma(m + m^*), \quad (\text{B6})$$

$$\dot{h} = -\gamma h, \quad (\text{B7})$$

where dots label time derivative with respect to τ . We have omitted the time dependence on the parameters for simplicity. In the equation, γ and κ are the total decay rate and difference in the decay rates between the qubits, defined in Eqs. (9) and (10), respectively.

The set of equations has the following solutions, where x, y and z are defined in Eqs. (6)–(8), respectively. In the following expressions, the subscript 0 denotes initial conditions,

$$a(\tau) = e^{-2\gamma\tau} a_0, \quad (\text{B8})$$

$$m(\tau) + m^*(\tau) = e^{-\gamma\tau} (m_0 + m_0^*), \quad (\text{B9})$$

$$h(\tau) = e^{-\gamma\tau} h_0, \quad (\text{B10})$$

$$\begin{aligned} x(\tau) &= -2a_0 \left[e^{-2\gamma\tau} - e^{-\gamma\tau} \left(1 - \frac{\kappa^2}{\Delta^2} (\cosh(\Delta\tau) - 1) \right) \right] + x_0 e^{-\gamma\tau} \left(1 - \frac{\kappa^2}{\Delta^2} (\cosh(\Delta\tau) - 1) \right) \\ &\quad + y_0 \frac{\kappa}{\Delta} e^{-\gamma\tau} \sinh(\Delta\tau) + z_0 \frac{i\kappa}{\Delta^2} e^{-\gamma\tau} (\cosh(\Delta\tau) - 1), \end{aligned} \quad (\text{B11})$$

$$y(\tau) = y_0 e^{-\gamma\tau} \cosh(\Delta\tau) + \left(a_0 \frac{2\kappa}{\Delta} + x_0 \frac{\kappa}{\Delta} + z_0 \frac{i}{\Delta} \right) e^{-\gamma\tau} \sinh(\Delta\tau), \quad (\text{B12})$$

$$z(\tau) = (2a_0 + x_0) \frac{i\kappa}{\Delta^2} e^{-\gamma\tau} (\cosh(\Delta\tau) - 1) + y_0 \frac{i}{\Delta} e^{-\gamma\tau} \sinh(\Delta\tau) + z_0 e^{-\gamma\tau} \left(1 - \frac{1}{\Delta^2} (\cosh(\Delta\tau) - 1) \right), \quad (\text{B13})$$

$$\begin{aligned} d(\tau) &= d_0 + a_0 \left[1 + e^{-2\gamma\tau} - 2e^{-\gamma\tau} \left(1 - \frac{\kappa^2}{\Delta^2} (\cosh(\Delta\tau) - 1) \right) \right] + x_0 \left[1 - e^{-\gamma\tau} \left(1 - \frac{\kappa^2}{\Delta^2} (\cosh(\Delta\tau) - 1) \right) \right] \\ &\quad - y_0 \frac{\kappa}{\Delta} e^{-\gamma\tau} \sinh(\Delta\tau) - z_0 \frac{i\kappa}{\Delta^2} e^{-\gamma\tau} (\cosh(\Delta\tau) - 1). \end{aligned} \quad (\text{B14})$$

Appendix C: Third-order exceptional points

In this appendix, we show that the five-parameter subspace represented by the vector $\mathbf{u} = (a, x, y, z, d)^T$, where

\mathbf{T} denotes matrix transpose, has two third-order exceptional points at $\kappa = \pm 1$. The matrix equation $\dot{\mathbf{u}} = \mathbf{L} \cdot \mathbf{u}$

has the non-Hermitian time evolution generator

$$\mathbf{L} \equiv \begin{pmatrix} -2\gamma & 0 & 0 & 0 & 0 \\ 2\gamma & -\gamma & \kappa & 0 & 0 \\ 2\kappa & \kappa & -\gamma & i & 0 \\ 0 & 0 & i & -\gamma & 0 \\ 0 & \gamma & -\kappa & 0 & 0 \end{pmatrix}. \quad (\text{C1})$$

It has the eigenvalues listed in Eq. (12), where λ_0 corresponds to the equilibrium state and Δ is defined in Eq. (13). The corresponding eigenvectors are

$$\mathbf{u}_0 = (0, 0, 0, 0, 1)^T, \quad (\text{C2})$$

$$\mathbf{u}_1 = (1, -2, 0, 0, 1)^T, \quad (\text{C3})$$

$$\mathbf{u}_2 = (0, 1, 0, i\kappa, -1)^T, \quad (\text{C4})$$

$$\mathbf{u}_3 = \pm(0, \kappa, -\Delta, i, -\kappa)^T, \quad (\text{C5})$$

$$\mathbf{u}_4 = \pm(0, \kappa, \Delta, i, -\kappa)^T, \quad (\text{C6})$$

where in \mathbf{u}_3 and \mathbf{u}_4 , we use the sign \pm when $\kappa = \pm 1$. By inspection, as $\kappa \rightarrow \pm 1$ at the exceptional points, $\mathbf{u}_2, \mathbf{u}_3$ and \mathbf{u}_4 coalesce into

$$\mathbf{u}_2 = \mathbf{u}_3 = \mathbf{u}_4 = (0, 1, 0, \pm i, -1)^T. \quad (\text{C7})$$

For non-Hermitian systems, we also need to consider the left-eigenvalue problem $\mathbf{L}^\dagger \cdot \mathbf{v} = \lambda \mathbf{v}$. The eigenvectors satisfy the biorthogonal relation $\mathbf{v}_i^\dagger \cdot \mathbf{u}_j = \delta_{ij}$ and the completeness relation $\sum_i \mathbf{u}_i \cdot \mathbf{v}_i^\dagger = I$, where i, j range from 0 to 4. We will not list the left eigenvectors here since this is not along the main theme of this work.

Appendix D: PT -symmetry and symmetry broken phase

In this appendix, we discuss the PT -symmetry phase transition of the two-qubit model across the exceptional points [2, 8]. To illustrate the phase transition, it is convenient to consider the expectation values of the four operators, $\langle \sigma_{\pm} \mu_{\pm} \rangle$, where we define $\langle O \rangle \equiv \text{tr}(O\rho)$, and O is a two-qubit operator. We calculate the time evolution of the operators by tracing out the operators with the GKSL master equation (2). In terms of the vector

$$\mathbf{q} \equiv (\langle \sigma_{+} \mu_{+} \rangle, \langle \sigma_{+} \mu_{-} \rangle, \langle \sigma_{-} \mu_{+} \rangle, \langle \sigma_{-} \mu_{-} \rangle)^T, \quad (\text{D1})$$

where T denotes matrix transpose, we obtain the equation of motion $d\mathbf{q}/d\tau = -\gamma \mathbf{q} - i\mathbf{M} \cdot \mathbf{q}$, where

$$\mathbf{M} \equiv \begin{pmatrix} i\kappa & \frac{1}{2} & -\frac{1}{2} & 0 \\ \frac{1}{2} & 0 & 0 & -\frac{1}{2} \\ -\frac{1}{2} & 0 & 0 & \frac{1}{2} \\ 0 & -\frac{1}{2} & \frac{1}{2} & -i\kappa \end{pmatrix} \quad (\text{D2})$$

is a time evolution matrix. Redefining the vector as $\bar{\mathbf{q}} \equiv \exp(\gamma\tau)\mathbf{q}$, which is called a gauge transformation

in Ref. [7], we obtain an explicit PT -symmetric equation of motion

$$i \frac{d}{d\tau} \bar{\mathbf{q}} = \mathbf{M} \cdot \bar{\mathbf{q}}. \quad (\text{D3})$$

To show that Eq. (D3) is indeed PT symmetric, we define the parity operator as $P \equiv \sigma_x \mu_x$, and the anti-linear time-reversal operator T is a complex conjugation operator with the action $TiT = -i$, and reverses the time $T\tau T = -\tau$. Furthermore, P and T commute $[P, T] = 0$ and they are their own inverse, $P^2 = I$ and $T^2 = I$, where I is the identity operator. We can now verify that \mathbf{M} is indeed PT symmetric

$$PT\mathbf{M}(PT)^{-1} = \mathbf{M}, \quad (\text{D4})$$

and Eq. (D3) shows this as well.

The eigenvalue problem $\mathbf{M} \cdot \mathbf{v} = \lambda \mathbf{v}$ has four solutions, $\lambda_1 = 0, \lambda_2 = 0, \lambda_3 = -\bar{\Delta}$, and $\lambda_4 = \bar{\Delta}$, where

$$\bar{\Delta} \equiv \sqrt{1 - \kappa^2}. \quad (\text{D5})$$

The corresponding eigenvectors are

$$\mathbf{v}_1 = \begin{pmatrix} 1 \\ -2ik \\ 0 \\ 1 \end{pmatrix}, \quad \mathbf{v}_2 = \begin{pmatrix} 0 \\ 1 \\ 1 \\ 0 \end{pmatrix}, \quad (\text{D6})$$

$$\mathbf{v}_3 = \begin{pmatrix} 1 - 2\bar{\Delta}^2 + 2ik\bar{\Delta} \\ \bar{\Delta} - i\kappa \\ -(\bar{\Delta} - i\kappa) \\ 1 \end{pmatrix}, \quad \mathbf{v}_4 = \begin{pmatrix} 1 - 2\bar{\Delta}^2 - 2ik\bar{\Delta} \\ -(\bar{\Delta} + i\kappa) \\ \bar{\Delta} + i\kappa \\ 1 \end{pmatrix}. \quad (\text{D7})$$

The eigenvalues are real when $|\kappa| < 1$. This is the PT -symmetric region where the eigenvalues are also PT -symmetric, i.e., $PT\lambda_i(PT)^{-1} = \lambda_i$, though \mathbf{v}_i may not be the eigenstates of the PT operator. Apart from an overall exponential decay, the motion has oscillatory behavior, $\mathbf{q}(\tau) = \exp(-\gamma\tau) \sum_i c_i \exp(-i\lambda_i\tau) \mathbf{v}_i$ with real λ_i , where we expand the initial condition in terms of the eigenvectors $\mathbf{q}(0) = \sum_i c_i \mathbf{v}_i$, and c_i 's are the expansion coefficients. This region is the analog of the underdamped motion of the damped oscillator discussed in App. A.

In the region $|k| > 1$, two of the eigenvalues $\lambda_{3,4}$ become imaginary $\lambda_3 = -i\Delta$ and $\lambda_4 = i\Delta$, where $\Delta = \sqrt{\kappa^2 - 1}$ (13). In this region, even though \mathbf{M} remain PT symmetric, two of the eigenvalues are not,

$$PT\lambda_{3,4}(PT)^{-1} = \lambda_{3,4}^* \neq \lambda_{3,4}, \quad (\text{D8})$$

i.e., the PT -symmetry of the solutions is spontaneously broken [2, 7]. The motion is now purely exponential, in analogy to the overdamped motion of a damped oscillator. The critical points where the transition between the PT -symmetry phase and spontaneously broken PT -symmetry phase occur are the exceptional points. In this model, they are $\kappa = \pm 1$. In this subspace of four operators, the exceptional points are of second order, in which the pair of eigenvalues λ_3 and λ_4 as well as the pair of eigenvectors \mathbf{v}_3 and \mathbf{v}_4 coalesce.

Appendix E: Instant of the first maximum concurrence

In this appendix we obtain the instant defined as τ'_{10} , when the first maximum concurrence of C_{10} is reached. The time derivative of the concurrence is

$$\frac{dC_{10}}{d\tau} = 2 \frac{|\kappa|}{\kappa^2 - 1} \left| \gamma + A \cosh(\Delta\tau) + B \sinh(\Delta\tau) \right|, \quad (\text{E1})$$

where

$$A = \frac{\Delta^2}{\kappa} - \gamma, \quad (\text{E2})$$

$$B = \left(1 - \frac{\gamma}{\kappa}\right) \Delta. \quad (\text{E3})$$

Solving $dC_{10}/d\tau|_{\tau=\tau'_{10}} = 0$ for the first maximum, we obtain for $1 < |\kappa|$,

$$\tanh(\tau'_{10}\Delta) = \frac{\gamma|\kappa|B \mp \Delta A \sqrt{1 + \gamma^2}}{\gamma|\kappa|A \mp \Delta B \sqrt{1 + \gamma^2}}, \quad (\text{E4})$$

where we choose the upper sign in Eq. (E4) for $1 < \kappa$, and the lower sign for $\kappa < -1$. For $-1 < \kappa < 1$, we have instead

$$\tan(\tau'_{10}\bar{\Delta}) = \frac{\gamma|\kappa|\bar{B} \mp \bar{\Delta} A \sqrt{1 + \gamma^2}}{\gamma|\kappa|A \pm \bar{\Delta} \bar{B} \sqrt{1 + \gamma^2}}, \quad (\text{E5})$$

$$\bar{B} \equiv \left(1 - \frac{\gamma}{\kappa}\right) \bar{\Delta}, \quad (\text{E6})$$

where $\bar{\Delta}$ is defined in Eq. (D5) and we choose the upper sign in Eq. (E5) for $-1 < \kappa < 0$ and the lower sign for $0 < \kappa < 1$. At the exceptional points, $\kappa = \pm 1$, we have a simple expression for the instant of the first maximum concurrence, given by

$$\tau'_{10,\pm} = \frac{1}{\gamma} \left(1 \mp \gamma \pm \sqrt{1 + \gamma^2}\right). \quad (\text{E7})$$

When the decay rates of both qubits are the same, i.e., $\kappa = 0$, Eq. (E5) goes into $\tan \tau'_{10} \rightarrow 1/\gamma$. The maximum concurrence then occurs at $\tau'_{10}|_{\kappa=0} = \tan^{-1}(1/\gamma)$. For fixed γ , τ'_{10} is largest when $\kappa = \gamma$, see the discussion in Sec. III. The overall maximum time is then reached in the limit $\gamma \rightarrow 0$, where

$$\tau'_{10,\max} \rightarrow \frac{\pi}{2}, \quad (\text{E8})$$

or equivalently, $t'_{10,\max} = \pi/4J$ (17). The result can be obtained from Eq. (E5) by first setting $\kappa = \gamma$. Then, we substitute $\bar{B} = 0$ so that Eq. (E5) goes into $\tan(\sqrt{1 - \gamma^2}\tau'_{10,\max}) = 1/\gamma^2$. In the limit $\gamma \rightarrow 0$, we arrive at Eq. (E8).

Appendix F: Correlation functions

In this appendix we show that the extremum behavior of the concurrence, C'_{11} , depicted in Fig. 5(a) for the initial condition of two excited qubits also shows up in the two-qubit correlation function $\langle \sigma_x \mu_y \rangle = \text{tr}(\sigma_x \mu_y \rho)$. The quantity is related to the off-diagonal component of the X state by

$$\langle \sigma_x \mu_y \rangle = -i(z - h + h^*). \quad (\text{F1})$$

For the initial condition with two excited qubits ρ_{11} , cf. the first paragraph of Sec. IV, since $h(t) = h^*(t) = 0$, it takes the form

$$\langle \sigma_x \mu_y \rangle = -iz = \frac{2\kappa}{\Delta^2} e^{-\gamma\tau} (\cosh \Delta\tau - 1), \quad (\text{F2})$$

where $\Delta = \sqrt{\kappa^2 - 1}$ is defined in Eq. (13). We can solve for the instant when the first maximum is reached, denoted by τ'_{xy} , from $d\langle \sigma_x \mu_y \rangle / d\tau|_{\tau=\tau'_{xy}} = 0$, to get

$$\coth\left(\frac{\Delta}{2}\tau'_{xy}\right) = \frac{\gamma}{\Delta}. \quad (\text{F3})$$

For the special case $\kappa = \gamma$, the first maximum $\langle \sigma_x \mu_y \rangle'$ as a function of γ has an extremum, see Fig. 7(a), which is far from the exceptional point. However, the instant, τ'_{xy} , at which the maximum is reached is a monotonically reducing function in γ , see Fig. 7(b). Figs. 7(a) and 7(b) exhibit slightly different behaviors from Figs. 5(a) and 5(b) because the concurrence C_{11} (18) not only depends on the correlation function differently compared to $\langle \sigma_x \mu_y \rangle$ (F1), it also depends on the diagonal components of the density matrix.

We note that $\langle \sigma_y \mu_x \rangle = i(z + h - h^*)$. For the initial condition ρ_{11} , $\langle \sigma_y \mu_x \rangle = -\langle \sigma_x \mu_y \rangle$. Therefore, the plot of the first extremum of $\langle \sigma_y \mu_x \rangle$, denoted by $\langle \sigma_y \mu_x \rangle'$, is the reflection of Fig. 7(a) along the horizontal γ axis, whereas the instant when the first extremum of $\langle \sigma_y \mu_x \rangle$ occurs, denoted by τ'_{yx} , gives the same plot as in Fig. 7(b).

Appendix G: Mixed states

For the mixed state $\rho_{\text{mix}}(\alpha)$ (20), substituting the initial conditions $a_0 = 1 - \alpha$, $x_0 = y_0 = \alpha$, and $c_0 = d_0 = z_0 = h_0 = 0$, into Eqs. (B8), (B13) and (B14), we obtain for $1 < |\kappa|$,

$$a(\tau) = (1 - \alpha)e^{-2\gamma\tau}, \quad (\text{G1})$$

$$z(\tau) = 2ie^{-\gamma\tau} \sinh^2\left(\frac{\Delta}{2}\tau\right) \left[(2 - \alpha) \frac{\kappa}{\Delta^2} + \frac{\alpha}{\Delta} \coth\left(\frac{\Delta}{2}\tau\right) \right], \quad (\text{G2})$$

$$\begin{aligned}
d(\tau) = & (1 - \alpha) \left[(1 - e^{-\gamma\tau})^2 - \frac{4\kappa^2}{\Delta^2} e^{-\gamma\tau} \sinh^2 \left(\frac{\Delta}{2} \tau \right) \right] \\
& + \alpha \left[1 - e^{-\gamma\tau} - 2e^{-\gamma\tau} \sinh^2 \left(\frac{\Delta}{2} \tau \right) \right. \\
& \left. \times \left(\frac{\kappa^2}{\Delta^2} + \frac{\kappa}{\Delta} \coth \left(\frac{\Delta}{2} \tau \right) \right) \right]. \quad (G3)
\end{aligned}$$

A corresponding expression for $-1 < \kappa < 1$ can be obtained using the identities of hyperbolic functions with imaginary arguments.

[1] C. M. Bender and S. Boettcher, Real spectra in non-hermitian hamiltonians having pt symmetry, *Phys. Rev. Lett.* **80**, 5243 (1998).

[2] C. M. Bender, D. C. Brody, and H. F. Jones, Complex extension of quantum mechanics, *Phys. Rev. Lett.* **89**, 270401 (2002).

[3] N. Moiseyev, *Non-Hermitian quantum mechanics* (Cambridge, New York, 2011).

[4] M. Naghiloo, M. Abbasi, Y. N. Joglekar, and K. W. Murch, Quantum state tomography across the exceptional point in a single dissipative qubit, *Nat. Phys.* **15**, 1232 (2019).

[5] W. Chen, M. Abbasi, Y. N. Joglekar, and K. W. Murch, Quantum jumps in the non-hermitian dynamics of a superconducting qubit, *Phys. Rev. Lett.* **127**, 140504 (2021).

[6] P.-R. Han, F. Wu, X.-J. Huang, H.-Z. Wu, C.-L. Zou, W. Yi, M. Zhang, H. Li, K. Xu, D. Zheng, H. Fan, J. Wen, Z.-B. Yang, and S.-B. Zheng, Exceptional entanglement phenomena: Non-hermiticity meeting non-classicality, *Phys. Rev. Lett.* **131**, 260201 (2023).

[7] S. K. Özdemir, S. Rotter, F. Nori, and L. Yang, Parity-time symmetry and exceptional points in photonics, *Nat. Mat.* **18**, 783 (2019).

[8] X. Zhang, Y. Ma, Q. Liu, N. Wang, Y. Jia, Q. Zhang, Z. Bai, J. Zhang, Q. Gong, and Y. Gu, \mathcal{PT} -phase diagram with quantum jump in a non-hermitian photonic structure, *Phys. Rev. A* **109**, L041503 (2024).

[9] C. E. Rüter, K. G. Makris, R. El-Ganainy, D. N. Christodoulides, M. Segev, and D. Kip, Observation of parity-time symmetry in optics, *Nat. Phys.* **6**, 192 (2010).

[10] M.-A. Miri and A. Alú, Exceptional points in optics and photonics, *Science* **363**, eaar7709 (2019).

[11] C. M. Bender, B. K. Berntson, D. Parker, and E. Samuel, Observation of pt phase transition in a simple mechanical system, *Am. J. Phys.* **81**, 173 (2013).

[12] X. Zhou, X. Ren, D. Xiao, J. Zhang, R. Huang, X. Li, Zhipeng Sun, X. Wu, C.-W. Qiu, F. Nori, and H. Jing, Higher-order singularities in phase-tracked electromechanical oscillators, *Nat. Commun.* **14**, 7944 (2023).

[13] M. Berry, Physics of nonhermitian degeneracies, *Czech. J. Phys.* **54**, 1039 (2004).

[14] W. D. Heiss, The physics of exceptional points, *J. Phys. A: Math. Theor.* **45**, 444016 (2012).

[15] G. Bhamathi and E. C. G. Sudarshan, Double resonances and jordan block spectra, *Int. J. Mod. Phys. B* **10**, 1531 (1996).

[16] A. Bohm, M. Loewe, S. Maxson, P. Patuleanu, C. Püntmann, and M. Gadella, Gamow-jordan vectors and non-reducible density operators from higher-order s-matrix poles, *J. Math. Phys.* **38**, 6072 (1997).

[17] S. H. Weintraub, *Jordan Canonical Form: Application to Differential Equations* (Morgan & Claypool, San Rafael, 2008).

[18] N. Hatano, Exceptional points of the lindblad operator of a two-level system, *Mol. Phys.* **117**, 2121 (2019).

[19] F. Minganti, A. Miranowicz, R. W. Chhajlany, and F. Nori, Quantum exceptional points of non-hermitian hamiltonians and liouvillians: The effects of quantum jumps, *Phys. Rev. A* **100**, 062131 (2019).

[20] W. Chen, M. Abbasi, B. Ha, S. Erdamar, Y. N. Joglekar, and K. W. Murch, Decoherence-induced exceptional points in a dissipative superconducting qubit, *Phys. Rev. Lett.* **128**, 110402 (2022).

[21] F. Minganti, A. Miranowicz, R. W. Chhajlany, I. I. Arkhipov, and F. Nori, Hybrid-liouvillian formalism connecting exceptional points of non-hermitian hamiltonians and liouvillians via postselection of quantum trajectories, *Phys. Rev. A* **101**, 062112 (2020).

[22] Z.-Z. Li, W. Chen, M. Abbasi, K. W. Murch, and K. B. Whaley, Speeding up entanglement generation by proximity to higher-order exceptional points, *Phys. Rev. Lett.* **131**, 100202 (2023).

[23] J. Zhang, Y.-L. Zhou, Y. Zuo, H. Zhang, P.-X. Chen, H. Jing, and L.-M. Kuang, Exceptional entanglement and quantum sensing with a parity-time-symmetric two-qubit system, *Adv. Quantum Technol.* **7**, 2300350 (2024).

[24] H. Xu, D. Mason, L. Jiang, and J. G. E. Harris, Topological energy transfer in an optomechanical system with exceptional points, *Nature* **537**, 80 (2016).

[25] S. Assawaworrarit, X. Yu, and S. Fan, Robust wireless power transfer using a nonlinear parity-time symmetric circuit, *Nature* **546**, 387 (2017).

[26] H. Hodaei, A. U. Hassan, S. Wittek, R. Garcia-Gracia, HipolitoEl-Ganainy, D. N. Christodoulides, and M. Khajavikhan, Enhanced sensitivity at higher-order exceptional points, *Nature* **548**, 187 (2017).

[27] W. Chen, S. Kaya Özdemir, G. Zhao, J. Wiersig, and L. Yang, Exceptional points enhance sensing in an optical microcavity, *Nature* **548**, 192 (2017).

[28] M. V. Berry and R. Uzdin, Slow non-hermitian cycling: exact solutions and the stokes phenomenon, *J. Phys. A: Math. Theor.* **44**, 435303 (2011).

[29] R. Uzdin, A. Mailybaev, and N. Moiseyev, On the observability and asymmetry of adiabatic state flips generated by exceptional points, *J. Phys. A: Math. Theor.* **44**, 435302 (2011).

[30] K. Sun and W. Yi, Chiral state transfer under dephasing, *Phys. Rev. A* **108**, 013302 (2023).

[31] J.-W. Zhang, J.-Q. Zhang, G.-Y. Ding, J.-C. Li, J.-T. Bu, B. Wang, L.-L. Yan, S.-L. Su, L. Chen, F. Nori, F. Özdemir, S.K. and Zhou, H. Jing, and M. Feng, Dynamical control of quantum heat engines using excep-

tional points, *Nat. Commun.* **13**, 6225 (2022).

[32] Y.-X. Zhang, Z.-T. Zhang, X.-Z. Wei, B.-L. Liang, F. Mei, and Z.-S. Yang, Entanglement dynamics of two non-hermitian qubits, *J. Phys. B* **57**, 085501 (2024).

[33] Z. Li, X. Huang, H. Zhu, G. Zhang, F. Wang, and X. Zhong, Multitype entanglement dynamics induced by exceptional points, *Phys. Rev. A* **111**, 022213 (2025).

[34] M. B. Plenio and S. F. Huelga, Dephasing-assisted transport: quantum networks and biomolecules, *New J. Phys.* **10**, 113019 (2008).

[35] A. W. Chin, A. Datta, F. Caruso, S. F. Huelga, and M. B. Plenio, Noise-assisted energy transfer in quantum networks and light-harvesting complexes, *New J. Phys.* **12**, 065002 (2010).

[36] A. W. Chin, S. F. Huelga, and M. B. Plenio, Coherence and decoherence in biological systems: principles of noise-assisted transport and the origin of long-lived coherences, *Philos. Trans. R. Soc., A* **370**, 3638 (2012).

[37] A. Hewgill, A. Ferraro, and G. De Chiara, Quantum correlations and thermodynamic performances of two-qubit engines with local and common baths, *Phys. Rev. A* **98**, 042102 (2018).

[38] L. Bresque, P. A. Camati, S. Rogers, K. Murch, A. N. Jordan, and A. Auffèves, Two-qubit engine fueled by entanglement and local measurements, *Phys. Rev. Lett.* **126**, 120605 (2021).

[39] J. Wiersig, Robustness of exceptional-point-based sensors against parametric noise: The role of hamiltonian and liouvillian degeneracies, *Phys. Rev. A* **101**, 053846 (2020).

[40] V. May and O. Kühn, *Charge and Energy Transfer Dynamics in Molecular Systems*, 3rd ed. (Wiley-VCH, Weinheim, 2011).

[41] M. A. Nielsen and I. L. Chuang, *Quantum Computation and Quantum Information* (Cambridge, New York, 2000).

[42] V. Gorini, A. Kossakowski, and E. C. G. Sudarshan, Completely positive dynamical semigroups of n -level systems, *J. Math. Phys.* **17**, 821 (1976).

[43] G. Lindblad, On the generators of quantum dynamical semigroups, *Commun. Math. Phys.* **48**, 119 (1976).

[44] T. Yu and J. H. Eberly, Finite-time disentanglement via spontaneous emission, *Phys. Rev. Lett.* **93**, 140404 (2004).

[45] T. Yu and J. Eberly, Entanglement evolution in a non-markovian environment, *Opt. Commun.* **283**, 676 (2010).

[46] S.-B. Zheng and G.-C. Guo, Efficient scheme for two-atom entanglement and quantum information processing in cavity qed, *Phys. Rev. Lett.* **85**, 2392 (2000).

[47] W. K. Wootters, Entanglement of formation of an arbitrary state of two qubits, *Phys. Rev. Lett.* **80**, 2245 (1998).